Modelling the effects of reservoir parameters and rock mineralogy on wettability during low salinity waterflooding in sandstone reservoirs

Motaz Saeed[a], Prashant Jadhawar[a,*], Subhash C. Ayirala[b], Rockey Abhishek [c], Yingfang Zhou[a]

[a] *School of Engineering, University of Aberdeen, Aberdeen AB24 3UE, Scotland, UK*

[b] *Upstream Advanced Research Center (EXPEC ARC), Saudi Aramco, Dhahran, Saudi Arabia*

[c] *Department of Energy and Petroleum Engineering, University of Stavanger, Stavanger, Norway*

1 Abstract

Low salinity waterflooding has been reported to yield incremental oil recovery from both field applications and laboratory experiments compared to regular waterflooding. Crude oil-brine-rock (COBR) interactions dictate wettability alteration during low salinity waterflooding in sandstones. In this work, triple-layer surface complexation modelling (TLM) is utilised to simulate the interactions at rock-brine and oil-brine interfaces, while accommodating the crucial role of sandstone mineralogy in surface chemistry. Derjaguin-Landau-Verwey-Overbeek (DLVO) theory is applied to characterise the COBR stability. Moreover, we propose the use of the maximum energy barrier (MEB) parameter, which is calculated from the DLVO theory's interaction potential, as an indicator of reservoir wettability.

Correlating the MEB with the experimentally measured contact angles revealed an abrupt increase in contact angles as the MEB drops below the zero-value thereby leading to a less water-wet COBR system. Results analyses showed that the different clays affect the rock-brine zeta potential and wettability distinctly based on their surface site densities and specific surface areas. And the studied clays cause the zeta potential to become more negative in the order: smectite > montmorillonite >

illite > chlorite > kaolinite. Subsequently, further investigation employing the developed TLM and MEB revealed that higher amounts of kaolinite will make the reservoir more oil-wet.

Lastly, the sensitivity analysis performed on reservoir wettability indicated that the ionic composition is the most important factor to affect rock wettability followed by pH and temperature. Moreover, the presence of $CaCl_2$ salt in the formation water significantly supresses the areas of strong water wettability under varying reservoir conditions compared to NaCl salt.

The work conducted in this study presents a novel approach to model the individual and combined effects of sandstone minerals, specifically, quartz, kaolinite, chlorite, illite, montmorillonite and smectite, on the overall sandstone zeta potential behaviour. Furthermore, a new method was proposed to characterise reservoir wettability as a function of the maximum energy barrier which allowed us to obtain valuable insights into the most affecting reservoir parameters on COBR wettability. These findings will have practical implications to efficiently design the low salinity waterflooding processes for sandstone reservoir applications.

Keywords*: Rock-Brine Interface, Sandstone Reservoirs, Wettability Alteration, Triple-layer Surface Complexation Modelling, Low Salinity Waterflooding*

2 Introduction

Incremental oil recovery by low salinity waterflooding (LSWF) has been observed in both experimental and field applications in the sandstone porous media and has been the focus of numerous research studies [1]. LSWF has gained significant attention in the past two decades since it is relatively cheap when compared to other conventional enhanced oil recovery technologies (EOR) relying on costly chemicals and solvents. It also does not need major modifications in producing facilities besides capitalizing on the waterflooding infrastructure already available in sandstone oil fields. The synergization of LSWF with chemicals (surfactant, polymer) and nanoparticles is also recently becoming popular due to the favourable effects of low salinity water to reduce chemical usage and achieve higher oil recoveries [2-5].

Several mechanisms have been suggested to be the reason behind LSWF incremental recoveries including the fines migration, multi-component ion exchange (MIE), double-layer expansion, and alkaline-like effect [6-10]. There is no common consensus on a single mechanism, and it is also most likely that a combination of these mechanisms may be in play depending on studied systems and conditions. Double-layer expansion is widely believed to play an important role in bringing out the favourable low salinity effect on changing the wettability of the porous medium via the ionic interactions at the oil-brine and rock-brine interfaces. This paper presents the nano-scale results of such interactions using a newly developed triple-layer surface complexation model (TLM) in the crude oil-brine-rock system relevant to a sandstone reservoir. Wettability alteration from oil-wet to water-wet conditions is believed to be a result of the double-layer expansion [11]. The charges at the oil-brine and rock-brine interfaces determine the thickness of thin water film between the oil and rock surfaces. Negative charges at both interfaces cause them to repulse, leading to the expansion of the thin water film thickness. Such expansion results in a more stable colloidal crude oil-brine-rock system in sandstones, where the rock surface is in more contact with brine than oil making the system water-wet. The interactions at the oil-brine and rock-brine interfaces depend on the brine composition as well as the surface-active functional groups at the oil and rock surfaces. The common surface-active groups on the oil surface are (-NH) and (-COOH), and on the sandstone rock surface are (>AlOH) and (>SiOH). These surface groups undergo protonation/deprotonation reactions and association/dissociation reactions with the potential determining ions (PDIs) present in the brine, which determines the oil and rock surface charges. More details on experimental evidence demonstrating how reservoir parameters dictate the COBR interactions and low salinity waterflooding performance in sandstone rocks can be found elsewhere [12].

Interactions at the oil-brine and rock-brine interfaces are simulated by the surface complexation models (SCM). Brady and Krumhansl [13] highlighted that diffuse double-layer (DDL) SCM can

74 be used to calculate the concentration of the electrostatic bridges connecting the oil and clay
75 surfaces, thus predicting the degree of oil adhesion before and after the LSWF. The electrostatic
76 bridges [13] are a result of a series of chemical reactions and electro-kinetic attraction forces. The
77 COBR system in their model included rock containing kaolinite clay, oil with functional groups
78 carboxylic ($-COOH^-$) and nitrogen bases ($-NH^+$) and divalent cations Ca^{2+} and Mg^{2+} in water. They
79 concluded that high concentrations of certain oppositely charged species such as [> $Al{:}Si{-}O^-$], [>
80 $Al{-}O{-}H_2^+$], [$-COOCa^+$], [$-COO^-$], [$-NH^+$] present on rock and oil surfaces, will lead to the
81 electrostatic attraction between the two surfaces resulting in the adhesion of oil to rock surface
82 (Figure 1). Details on the other oil-brine and rock-brine DDL-SCMs for both sandstone and
83 carbonate rocks have been reported elsewhere [14-21].

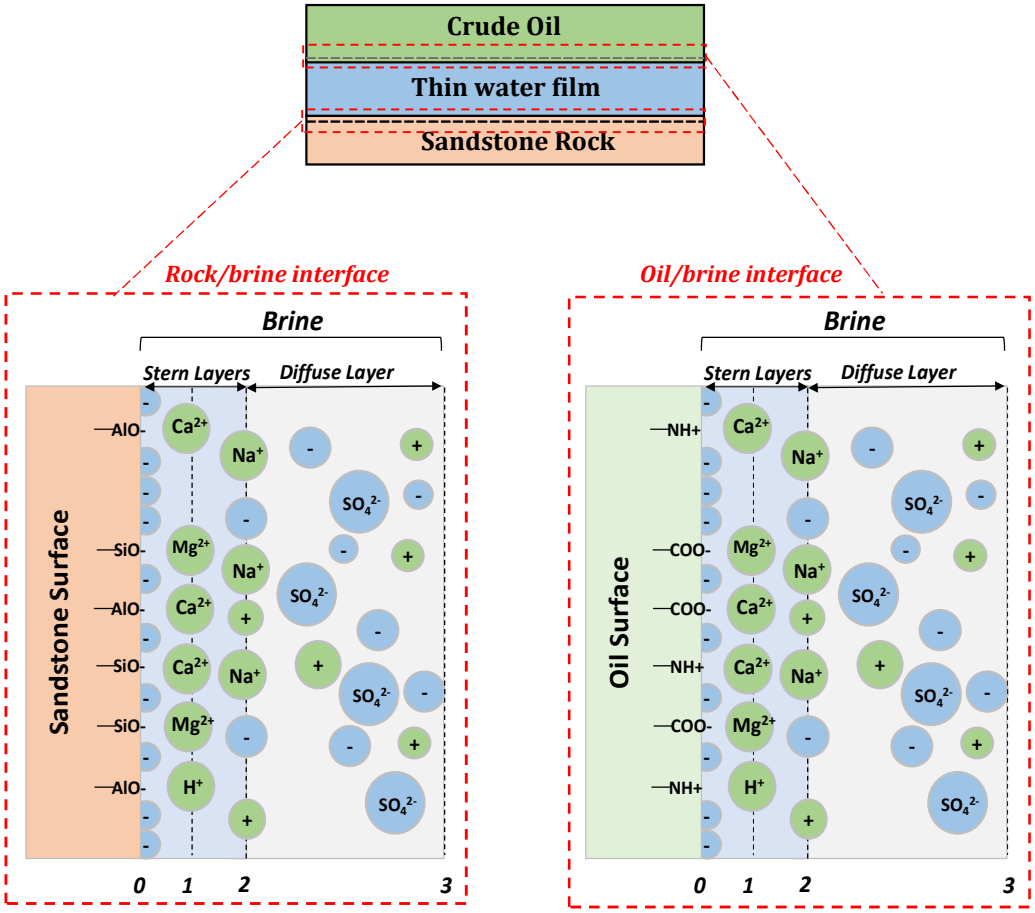

84

85 **Figure 1 (top) Representation of thin water film between oil/brine and rock/brine interfaces,**

86 **(bottom) Representation of the sandstone-brine and oil-brine electrical interfacial layers**

87 On the other hand, triple-layer surface complexation models (TLMs) include three adsorption
88 layers rather than two layers which is the case in double-layer models (see Figure 1). The layers in
89 a TLM are the inner Helmholtz layer constrained by the electrostatic planes 0- and 1-planes, the
90 outer Helmholtz layer between the 1- and 2-planes and the diffuse layer extending from the 2-plane
91 to 3-plane. The inner and outer Helmholtz layers are known as the Stern layers as depicted in Figure
92 1. Moreover, TLM enables the modelling of inner and outer Helmholtz layer complexes and the
93 charge distribution of the adsorbed potential determining ions between the different electrostatic
94 planes leading to a better representation of the electrical interfacial layers [22-24]. A few triple-
95 layer surface complexation models (TLM) were developed to describe sandstone rock-brine
96 interfaces [25-31]. Most of these previous TLMs used single minerals such as quartz and kaolinite

97 to describe the rock surface. However, the other clay minerals such as illite, chlorite, smectite,
98 montmorillonite, muscovite etc. are present in the sandstone and other clays. The individual and
99 combined effect of these other minerals on the overall surface charge and zeta potential in
100 sandstone rock systems were not accommodated in those investigated TLMs, which can be
101 considered as the most important limitation of previously reported models in the existing
102 knowledge.
103 The mineralogy of sandstone affects the wetting condition in the crude oil-brine-rock system
104 [11,13]. The sandstone rock surface chemistry is the resultant of the protonation/deprotonation and
105 cation/anion sorption reactions of the mineral surface groups. The clay surface charge can be
106 defined as the sum of the edge plane and basal plane charges. In this work, we consider only the
107 edge plane charge which is controlled mainly by the surface groups Aluminol (>AlOH) and Silanol
108 (>SiOH). In addition to the surface groups, clay surface charge is also dictated by the clay specific
109 surface area, temperature, brine salinity and pH [13,32]. Different clay minerals such as kaolinite,
110 illite and chlorite have different surface group site densities and specific surface areas. These
111 differences result in distinct surface charge behaviour for the individual clays and their overall
112 contribution to the sandstone rock surface charge [33,34].
113 In the present study, we build upon our findings from a previously published work [35] utilising
114 the newly developed oil-brine TLM, by integrating it with the sandstone-brine interfacial TLM
115 (this work) to evaluate the effect of different clay minerals. These clay minerals include kaolinite,
116 illite, chlorite, montmorillonite and smectite (in addition to quartz), which represent a considerable
117 portion of the overall sandstone rock mineralogy [36]. The values of the >AlOH and >SiOH surface
118 site densities and clay specific area for the modelled sandstone minerals were extracted from
119 various published experimental and modelling studies, as summarised in Table 1.
120 The novelty of work undertaken in this investigation lies in (i) the inclusion of the individual and
121 combined effects of different reservoir minerals, specifically quartz, kaolinite, chlorite, illite,

montmorillonite and smectite, on the surface charge behaviour at sandstone surface and (ii) development of the correlation between the maximum energy barrier, (defined as the maximum of the DLVO theory's interaction potential energy curve [37]) contact angles and reservoir wettability in different crude oil-brine-sandstone rock systems.

The following section will present the methodology adopted in this work. Subsequently, the results of sandstone-brine interface model validation and zeta potential sensitivity analysis are discussed. Later, wettability correlation with the maximum energy barrier parameter is presented followed by sensitivity analysis of COBR wettability to various reservoir parameters.

Table 1 Specific surface area and surface site density for sandstone minerals modelled in this work

Mineral	Specific surface area (g/m^2)		Surface site density ($site/nm^2$)		
	Value	Reference	>AlOH	>SiOH	Reference
Kaolinite	12	[38]	5.5	5.5	[33,38]
Chlorite	2.4	[38]	5.5	5.5	This study
Illite	22.3	[39]	≈2.6	≈5.3	[34]
Montmorillonite	71	[38]	≈1	≈2	[40]
Smectite	31	[41]	≈0.6	≈0.6	[41]
Quartz	0.426	[42]	-	10	[43]

3 Methodology

The methodology adopted to develop the triple-layer surface complexation model describing the sandstone-brine interfacial interactions is presented. The developed sandstone-brine TLM was then validated and employed to assess the impact of rock mineralogy, salinity, and pH on the rock-brine zeta potential. The validated sandstone-brine interface model is further integrated with our previously reported oil-brine TLM [35] and the Derjaguin, Landau, Verwey, and Overbeek (DLVO) theory [44] to understand film stability and reservoir wettability alteration during the LSWF.

3.1 Sandstone Rock-Brine Triple-Layer Surface Complexation Model (TLM)

A sandstone rock-brine TLM was developed using the Donnan approach in CD-MUSIC, a module of the geochemical code PHREEQC^{TM} [45]. This TLM simulates the interactions at the rock-brine interface while taking account of the following parameters: inner and outer-Helmholtz layer capacitances, protonation/deprotonation and association/dissociation reactions equilibrium constants, surface site densities, specific surface areas and charge distribution. The assumptions made during this TLM development were: (i) quartz, kaolinite, illite, chlorite, montmorillonite and smectite are the most abundant minerals in the sandstone reservoir, hence their individual behaviour governs the overall sandstone surface charge behaviour; (ii) the overall average behaviour can be predicted by weight-averaging the specific surface area and surface site densities for each mineral; and (iii) the surface site density of chlorite is same as kaolinite due to a lack of data in the published literature. The results obtained from triple-layer modelling were validated against the reported experimental data (see Table 2) available in the literature.

Table 2 Summary of experimental conditions used for the published zeta potential data at the sandstone-brine interface

Reference	Rock Sample	Brine Electrolyte	Brine Salinity	pH	Temperature (°C)
[46]	Berea Sandstone	NaCl, $CaCl_2$	1500 ppm	2 to 11	25
[47]	Sandstone	NaCl, $CaCl_2$, $MgCl_2$	0.1 - 5 wt.%	7.3 to 9	25
[48]	Kaolinite, Montmorillonite	NaCl, $CaCl_2$	0.05 - 0.3 wt%	6.05 to 6.83	Room Temperature
[49]	Kaolinite	$CaCl_2$, $MgCl_2$	50 - 500 mmol/L	1.8 to 7.8	25
[50]	Sandstone	NaCl	0.2 - 10 wt.%	7.1 to 8.4	65
[51]	Berea Sandstone, Scioto Sandstone	Deionized Water, Aquifer Water, Seawater	5,436 - 174,156 mg/L	7.29 to 7.84	25
[52]	Kaolinite	NaCl	0.02 mol/L	3 to 11	25
[53]	Kaolinite	NaCl	0.0001 - 0.01 mol/L	3 to 11	25

The surface groups of minerals used are Aluminol (>AlOH) and Silanol (>SiOH). The potential determining ions (PDIs) modelled in the brine are calcium, magnesium, sodium, hydroxyl and hydrogen ions. The effect of sulphate ions in brine on zeta potential at the rock-brine interface is also evaluated in the model. The sodium ion forms an outer-sphere complex with the surface groups (>Al:SiOH) with its charge distributed between the 1- and 2-planes, while the calcium and magnesium ions form inner-sphere complexes with (>Al:SiOH) and have their charges on the 1-plane [23,54].

For pure individual clay minerals, the values of specific surface areas and surface site densities for >Al:SiOH, reported in Table 1, were directly used in the model to evaluate the rock-brine interactions. In modelling the surface of a sandstone rock comprising multiple minerals, the

weighted-average values of the surface site densities and specific surface area were employed. The specific surface area (SSA_{avg}) used in the model was averaged by the mineral weight/volume % in the overall sandstone rock mineralogy as shown in Eq. (1)

$$SSA_{avg} = \sum_i SSA_i \times wt_i\%(or\ vol_i\%) \quad \text{Eq. 1}$$

where SSA is the specific surface area and i denotes the mineral type. The surface site densities (N_s) for >AlOH and >SiOH were averaged based on both mineral weight/volume % in the overall sandstone rock mineralogy and the specific surface area of each mineral, using the following equation:

$$N_{s,avg} = \frac{\sum_i N_{s,i} \times SSA_i \times wt_i\%(or\ vol_i\%)}{SSA_{avg}} \quad \text{Eq. 2}$$

The capacitances (see Table 3) of the inner and outer Helmholtz layers determine the potential drop across the layer. These are dependent on the dielectric constant of the electrolyte and the distance between the planes. The detailed procedure for calculating the capacitance for each layer can be found in Saeed et al. [35]. The thickness of the diffuse layer was assumed to be twice the screening Debye length [34]. The inverse Debye length is calculated as follows:

$$k^{-1} = \sqrt{\frac{\varepsilon_o \varepsilon_r k_B T}{2000 N_A e^2 I}} \quad \text{Eq. 3}$$

where k_B is the Boltzmann constant, T is the absolute temperature, N_A is Avogadro's number, e is the electron charge, and I is the ionic strength of the solution.

3.1.1 Optimization of the sandstone Rock-Brine TLM

The association/disassociation equilibrium constants of the surface groups, >AlOH and >SiOH, were optimized to converge between the modelling and experimental zeta potential values. The modelling optimization process, illustrated in Figure 2, follows the optimization process described by Saeed et al. [35]. The experimental data required for the modelling run are brine composition, pH, temperature and sandstone rock mineralogy to calculate the average specific surface area for

the rock and average surface site densities of >AlOH and >SiOH. The optimized surface complexation reactions constants are shown in Table 3 along with the reactions' enthalpy, the charge distribution of the modelled PDIs and the capacitances of the inner and outer Helmholtz layers.

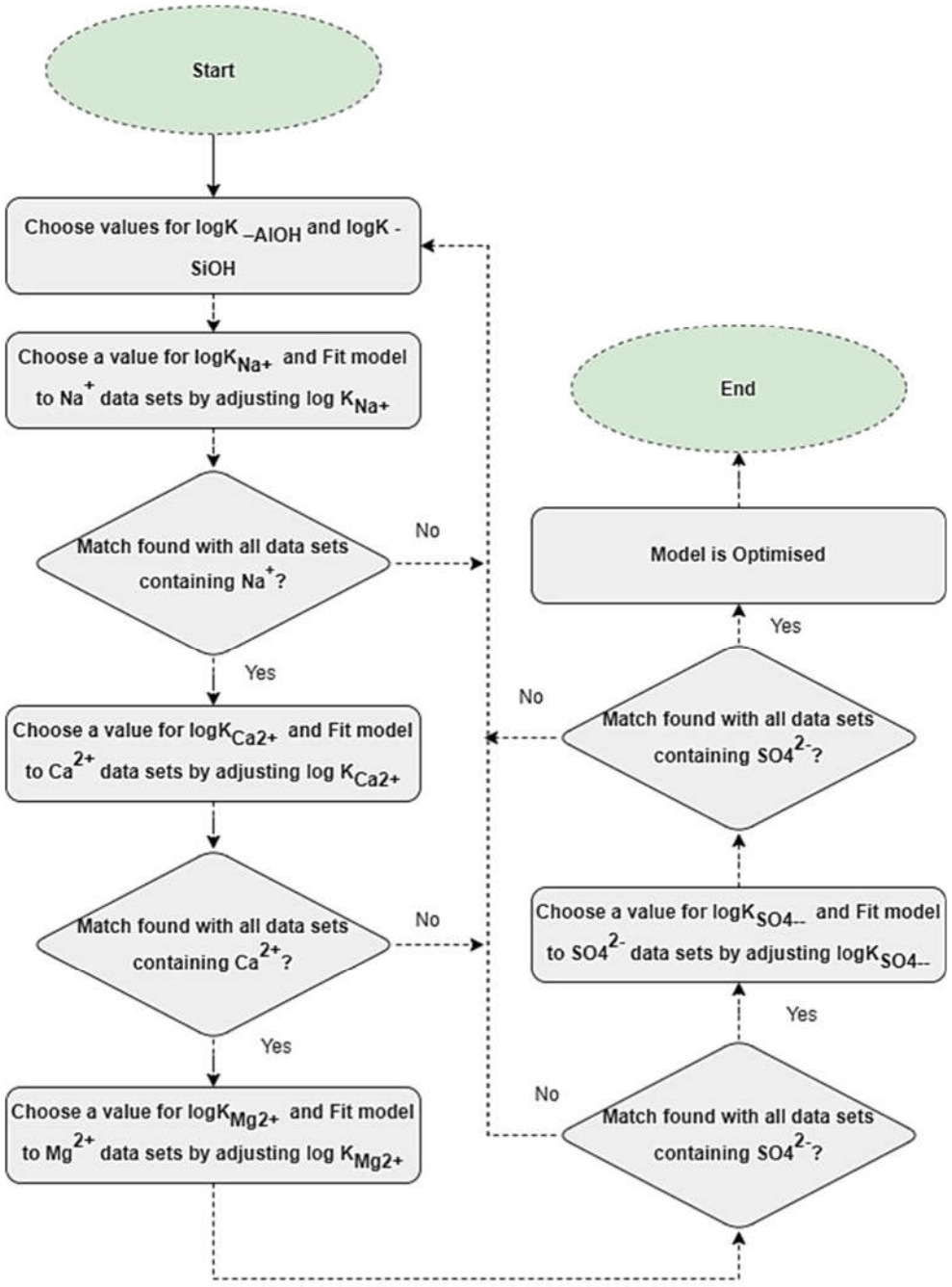

Figure 2 Sandstone rock-brine TLM optimization process flowchart

Table 3 Association/disassociation equilibrium constants, charge distribution and capacitance values optimised in this study for the developed sandstone-brine TLM

Surface Complexation Reaction	Log K @ 25° C	Enthalpy (kJ/mol)	Charge Distribution			C_1 (F/m^2)	C_2 (F/m^2)
			0-plane	1-plane	2-plane		
$>AlOH + H^+ \leftrightarrow\ > AlOH_2{}^+$	0.8	-5	+1	0	0	2.57	2.57
$>AlOH \leftrightarrow\ > AlO- + H^+$	-7.5	-40	-1	0	0	2.57	2.57
$>AlOH + Na^+ \leftrightarrow\ > AlONa + H^+$	-4.5	-60	-1	+0.5	+0.5	2.57	2.57
$>AlOH + Ca^{2+} \leftrightarrow\ > AlOCa^+ + H^+$	-3.5	-50	-1	+2	0	3.54	2.57
$>AlOH + Mg^{2+} \leftrightarrow\ > AlOMg^+ + H^+$	-3.5	-50	-1	+2	0	4.92	2.57
$>AlOH + SO_4{}^{2-} \leftrightarrow\ > AlO^- + HSO_4{}^-$	-1.5	-	-1	0	0	2.57	2.57
$>SiOH \leftrightarrow\ > SiO- + H^+$	-6.5	-40	-1	0	0	2.57	2.57
$>SiOH + Na^+ \leftrightarrow\ > SiONa + H^+$	-2	-60	-1	+0.5	+0.5	2.57	2.57
$>SiOH + Ca^{2+} \leftrightarrow\ > SiOCa^+ + H^+$	-2.5	-50	-1	+2	0	3.54	2.57
$>SiOH + Mg^{2+} \leftrightarrow\ > SiOMg^+ + H^+$	-2.8	-50	-1	+2	0	4.92	2.57
$>SiOH + SO_4{}^{2-} \leftrightarrow\ > SiO^- + HSO_4{}^-$	-1.5	-	-1	0	0	2.57	2.57

The sandstone-brine TLM developed in this study overcomes the limitations of previously reported sandstone rock-brine SCMs and TLMs [25-31]. The developed TLM successfully incorporates the individual and combined effects of the most abundant clays and minerals present in sandstone rocks, thereby providing an improved ability to quantify the impact of each clay on the overall zeta potential and reservoir wettability. The model was found to be effective in describing the adsorption of various PDIs i.e. H^+, Na^+, $Ca^{2+}$and Mg^{2+}, on the inner and outer Helmholtz layers of the sandstone rock-brine interface. The model also describes the effect of sulphate ions present in brine on the sandstone rock-brine interface.

3.2 Oil-brine interface TLM

Our previously reported oil-brine TLM [35] is integrated with the sandstone-brine TLM developed in this study, to evaluate the complete Crude Oil Brine Rock (COBR) system. The stability of the COBR was characterised using the DLVO theory calculations. The association/disassociation reaction equilibrium constants, charge distribution and capacitance were also considered in this study. The oil-brine TLM incorporates the effects of both the acidic and basic groups i.e. (-COOH) and (-NH), on the oil surface, and the adsorption/desorption of the PDIs, Na^+, Ca^{2+}, Mg^{2+} and H^+, on the oil surface groups. More details on the adopted oil-brine TLM can be found in [35].

3.3 Disjoining Pressure Calculations and Film Stability

The crude oil-brine-rock (COBR) system is analysed by calculating the disjoining pressure using the DLVO theory. The calculation of disjoining pressure requires the knowledge of zeta potentials at the oil-brine and rock-brine interfaces. These zeta potential values are adapted from the simulation output of the developed TLM and the geochemical code PHREEQC. The disjoining pressure can be calculated as the sum of two repulsive forces and an attractive force. The two repulsive forces are the electrical double-layer force and the structural force, while the attractive force is the Van der Waals force. To calculate the disjoining pressure, the individual forces are calculated and added together to find the net force acting between the oil-brine and rock-brine interfaces.

$$\Pi(h) = \Pi_{VdW}(h) + \Pi_{structural}(h) + \Pi_{electric}(h) \qquad \textit{Eq 4}$$

The Van der Waals forces between two plates including the retardation effects are calculated according to the following formula [55]:

$$\Pi_{VdW}(h) = -\frac{A\,(15.96\left(\frac{h}{\lambda_{lw}}\right) + 2)}{12\pi h^3(1 + 5.32\left(\frac{h}{\lambda_{lw}}\right))^2} \qquad \textit{Eq 5}$$

where, λ_{lw} is the London wavelength and is assumed to be 100 nm [55], h is the distance between the two interfaces and A is the Hamaker constant, obtained through [44]:

$$A = A_{v=0}(\kappa h)\exp(-2\kappa h) + A_{v>0} \qquad \textit{Eq 6}$$

where κ is the Debye-Huckel parameter, $A_{v=0}$ and $A_{v>0}$ are the contributions to Hamaker constant at zero and finite frequencies, respectively obtained using the following equations [44]:

$$A_{v=0} = \frac{3}{4}kT\left(\frac{\varepsilon_1-\varepsilon_3}{\varepsilon_1+\varepsilon_3}\right)\left(\frac{\varepsilon_2-\varepsilon_3}{\varepsilon_2+\varepsilon_3}\right) \qquad \textit{Eq 7}$$

$$A_{v>0} \approx \frac{3hv_e}{8\sqrt{2}}\frac{(n_1^2-n_3^2)(n_2^2-n_3^2)}{(n_1^2+n_3^2)^{0.5}(n_2^2+n_3^2)^{0.5}\{(n_1^2+n_3^2)^{0.5}+(n_2^2+n_3^2)^{0.5}\}} \qquad \textit{Eq 8}$$

where ε_1, $\varepsilon_2$and ε_3 are the dielectric constants for medium 1, 2 and 3, as considered in our case for hydrocarbons, quartz and water, respectively. n_1, n_2 and n_3 are the refractive indexes for medium 1, 2 and 3, respectively. The values for these parameters to calculate the Hamaker constant can be found in [44]. The structural forces are effective at low separation distances between the two interfaces < 5nm [56] and are calculated as follows:

$$\Pi_{structural}(h) = A_s e^{-\frac{h}{h_s}} \qquad \textit{Eq 9}$$

where A_s is a coefficient, assumed to be 1.5x10^{10} Pa [37] and h_s is the characteristic length, assigned the value of 0.05 nm [37].

For the two charged surfaces approaching each other, the two solutions for the Poisson-Boltzmann equation can be obtained using two different conditions [37,55,57]. One solution is the constant potential solution, and the other is the constant capacitance charge. It is predicted that a solution between them occurs. In this work, it is assumed that a constant potential solution [58] applies to simplify our calculations. Hence, the force resulting from the interaction of the two charged surfaces of oil and sandstone can be calculated by

$$\Pi_{electric}(h) = n_b k_b T \left(\frac{2\psi_{r1}\psi_{r2}\cosh(\kappa h) - {\psi_{r1}}^2 - {\psi_{r2}}^2}{[\sinh(\kappa h)]^2} \right) \qquad \textit{Eq 10}$$

where n_b is the ion density in the bulk solution, k_b is the Boltzmann constant (1.38×10^{-23} J/K), ψ_{r1} and ψ_{r2} are the reduced surface potentials for the rock-brine and oil-brine interfaces, respectively, and κ is the Debye-Hückel reciprocal length. The reduced potential can be calculated as follows:

$$\psi_r = \frac{ze\zeta}{kT} \qquad \textit{Eq 11}$$

where ζ is the zeta potential at the interface of interest. The specific interaction potential energy between two phases interacting through a third phase can be calculated as follows [37]

$$\omega = \int_h^{h_{eq}} (\Pi - \Pi_{eq}).\, dh \qquad \textit{Eq 12}$$

where h_{eq} and Π_{eq} are the separation distance and disjoining pressure at equilibrium conditions. The stability of the COBR system is directly related to the maximum interaction potential energy barrier (MEB), below which the VdW forces become dominant and the colloid falls into an unstable region and is destroyed [559].

In this work, we propose the use of MEB as the main indicator for film stability, and hence the wettability of the reservoir under investigation. The maximum energy barrier is calculated as the maximum of the interaction potential curve. To understand the effects of various reservoir parameters on the oil-brine-sandstone rock system's stability and wettability, the MEB is evaluated for several cases by varying the studied reservoir parameters. The MEB is calculated at zero capillary pressure in all the studied cases. Capillary pressure does affect the reservoir's wettability, however, setting its value to zero eliminates its effects on wettability and therefore focuses the investigation on the basis of brine, oil and rock compositions, pH and temperature only. For this application, we observe that the maximum energy barrier for the modelled cases ranges at film thicknesses between 0.5 and 1.5 nm. Hence, for consistency, we calculate the maximum of the interaction potential at this range for all the studied cases. With a higher MEB, the oil-brine-

sandstone system is more stable, and thus more water wet. As the MEB decreases, the stability of the oil-brine-sandstone system becomes less stable and less water-wet. The factors affecting the oil-brine-sandstone system's wettability include pH, temperature, salinity, oil TAN and TBN, and rock mineralogy among others. The first step in calculating the interaction potential energy is to model the oil-brine and rock-brine zeta potentials. The disjoining pressure is calculated according to *Eq 4*. Interaction potential is calculated using *Eq 12*. Finally, sensitivity analysis was utilised to evaluate the sensitivity of COBR wettability to changes in oil TAN and TBN, sandstone rock's average rock site density, brine composition, pH and temperature. This eventually enabled us to produce wettability maps for NaCl and $CaCl_2$ systems to further understand the importance of each parameter on wettability determination during the low salinity waterflooding process in sandstone reservoirs.

4 Results and Discussion

The published data sets of zeta potential measurements using brines and sandstone rock (see Table 2) were first extracted and then used to calibrate and validate the developed triple-layer model (TLM). The extracted datasets composed of experimental results performed under varying brines, sandstone mineralogical composition, pH, and temperatures. The correlation analysis between the calculated MEB and experimentally measured contact angles was performed. Results of sensitivity analysis are reported and discussed to evaluate the importance of the various parameters in dictating the zeta potential of a sandstone-brine interface and the sandstone reservoir wettability.

4.1 Sandstone-brine Triple-layer Model Validation

The developed model is validated, against the experimental datasets as detailed in Table 2. The validation was carried out by comparing the experimentally measured zeta potential with the model-predicted zeta potential values.

4.1.1 Modelling the zeta potential of pure clays

The experimental data from Yukselen-Aksoy and Kaya [52] were used to validate and calibrate the model developed in this work. Yukselen-Aksoy and Kaya used kaolinite as the rock sample and NaCl as the background electrolyte with a concentration of 0.02 M NaCl. The zeta potential was predicted for a pH range of 3 to 11 and at 25 °C temperature. The TLM simulation results (Figure 3) display the capability of the model to predict the trend of the zeta potential change with pH in the studied range. The results indicate that an increase in the pH value leads to higher negative zeta potential values which can be attributed to the enhancement of Al:SiOH deprotonation. This deprotonation causes the increase of the negatively charged Al:SiO- surface groups which progressively charge the kaolinite surface with a negative charge. The values of zeta potential calculated by the TLM were in close agreement with the experimental values except at pH between 5.0-6.8 where discrepancies are apparent, and the accuracy of the model drops to the range 76% - 82% which highlights some slight inaccuracy in modelling.

The effect of NaCl and $CaCl_2$ electrolyte on the zeta potential at the pure clay-brine surface was evaluated in this study using the experimental data extracted from Bazyari et al. [48]. The TLM was used to predict the zeta potential values at the rock-brine interface for two different types of pure clay minerals - kaolinite and montmorillonite. The TLM predicted results are matched with the experimental results reported [48] (see Figure 3). The model was able to closely predict the zeta potential values. It can also be seen that $CaCl_2$ electrolytes caused the zeta potential to be less positive for both kaolinite and montmorillonite in contrast to the NaCl electrolyte effect. This is attributed to the presence of the divalent cation Ca^{2+} which causes higher electrical screening to the negative charge present on the clay surfaces. The model shows accuracy ranging between 73% and 91% for the studied cases. The model exhibits better accuracy in predicting zeta potential in higher ionic strength electrolytes. This can be explained by the fact that higher ionic strength leads to

suppressing the zeta potential values, thereby minimising the discrepancies between model and measured zeta potentials.

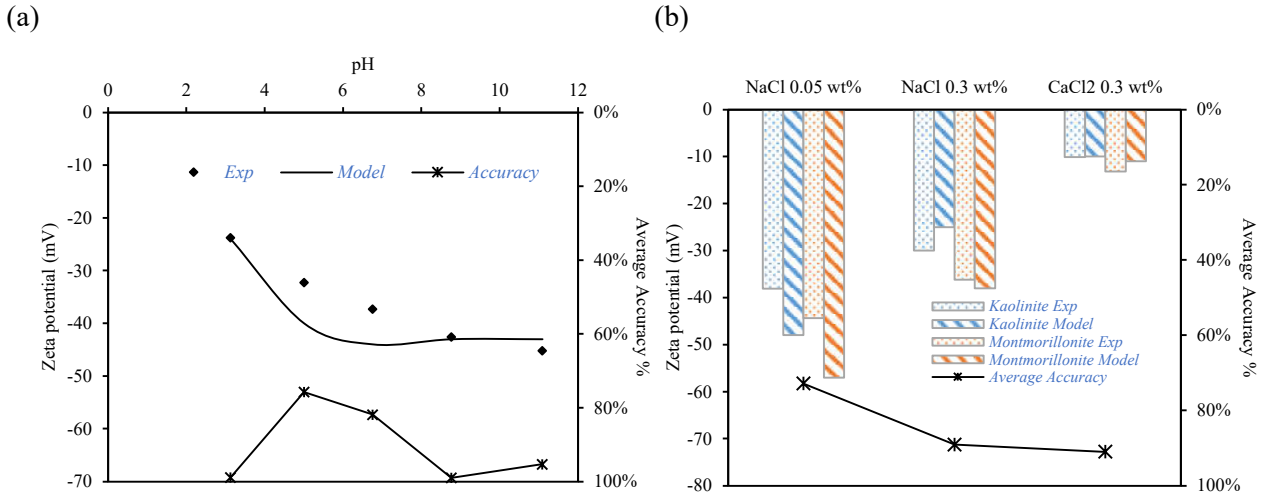

Figure 3 Experimental and modelling zeta potential values for (Left) Kaolinite [52] and (Right) kaolinite and montmorillonite [53]

4.1.2 Modelling the zeta potential of sandstone rocks

The rock-brine TLM proposed in our work was also used to replicate the experimental results of Farooq et al. [46] who studied the effect of varying cationic valences and pH conditions on an outcrop Berea sandstone sample. All their experiments were conducted at 25°C temperature conditions. The Berea sandstone sample mineralogy was used to calculate the rock properties required as input parameters of the TLM: average >Al:SiOH site density and average specific surface area using Eq. 1 and Eq. 2. Then the model was run to predict the zeta potential of the two cases using 1500 ppm and 1500 ppm electrolyte concentrations of NaCl and $CaCl_2$, respectively. The capacitance of the first layer parameter was varied according to the type of electrolyte used, 2.57 and 3.54 F/m^2 for NaCl and $CaCl_2$ in that order. For all cases, the second layer capacitance was fixed at a value of 2.57 F/m^2.

The model results and their comparison with the experimentally reported zeta potentials are shown in Figure 4a. The model successfully predicts the zeta potential for the Berea sandstone sample

within close proximity in both NaCl and $CaCl_2$ electrolytes. In addition, the model also provided accurate zeta potential predictions at high and low pH values with only small discrepancies at higher pH values. The model accuracy ranged between the average 73% and 97% averaged for both electrolytes containing Na^+ and Ca^{2+} respectively.

The developed sandstone-brine model was also tested against its ability to capture the effect of various clays present in the sandstone rock sample. Alotaibi et al. [51] focused on using Berea and Scioto sandstone samples in different electrolytes including deionized water, aquifer water and seawater. The salinity of the different electrolytes in addition to the mineralogy of the two rock samples were used in the developed model to calculate the zeta potential. Figure 4b presents both the experimental and modelling results as calculated from the TLM. The results demonstrate the ability of the model to give an accurate prediction of the zeta potential for both Berea and Scioto sandstone (Figure 4b) in deionized water and aquifer water with accuracies of 85% and 81%, respectively. However, there is distortion in modelling the seawater experiments which can be attributed to its considerably higher concentration of ions, and the different types of ions that are not included in this model. This has led the model to have a lower accuracy of about 70%. It is expected that incorporating the adsorption of more ions on the inner and outer Helmholtz layers would increase the model accuracy, especially in such cases where seawater is used as an electrolyte.

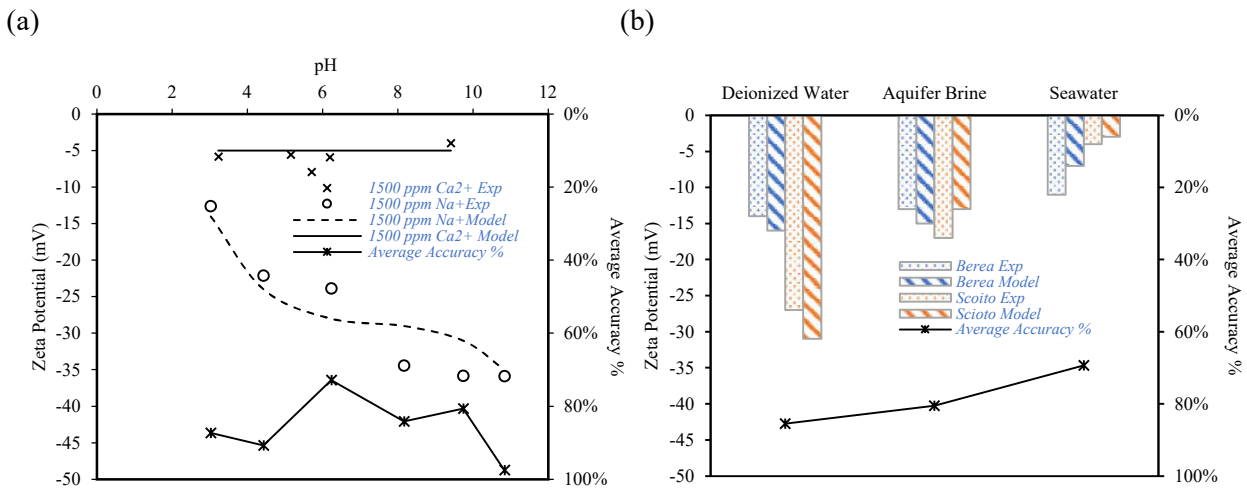

Figure 4 Experimental and modelling zeta potential values for (a) Berea sandstone [46] and (b) Berea sandstone sample and Scioto sandstone sample [51]

4.2 Wettability, film stability and the maximum energy barrier

First, we test the hypothesis that the maximum energy barrier is an indicator of reservoir wettability. The maximum of the interaction potential curve was calculated for several published experimental datasets [11, 17, 50, 59 – 61] obtained using different sandstone samples, reservoir minerals, oil composition, brine composition and temperature conditions. The MEB values was calculated from the zeta potential measurements reported in these published experimental datasets. The results were then fitted with the measured contact angles, as shown in Figure 5. Reservoir wettability is defined by the contact angle with the range 0° to 40° being strong water-wet, 40° to 65° as intermediate water-wet and 65° to 90° as weak water-wet. Figure 5 shows that as the MEB decreases from 0.07 to zero, the contact angle increases from 20º to 32º. However, this increase in the contact angle is sharper when MEB goes into negative. Such observation indicates that a small reduction in the MEB below zero-value increases the contact angle sharply, thereby causing the system to become less water wet (intermediate water-wet). The data depicted in Figure 5 clearly show two trends, one below zero MEB where the reservoir wettability abruptly becomes weaker with the decrease in the

MEB. While above zero MEB, the reservoir tends to stay in the strong water-wet region. These results validate our hypothesis that the MEB can be used as an indicator of reservoir wettability.

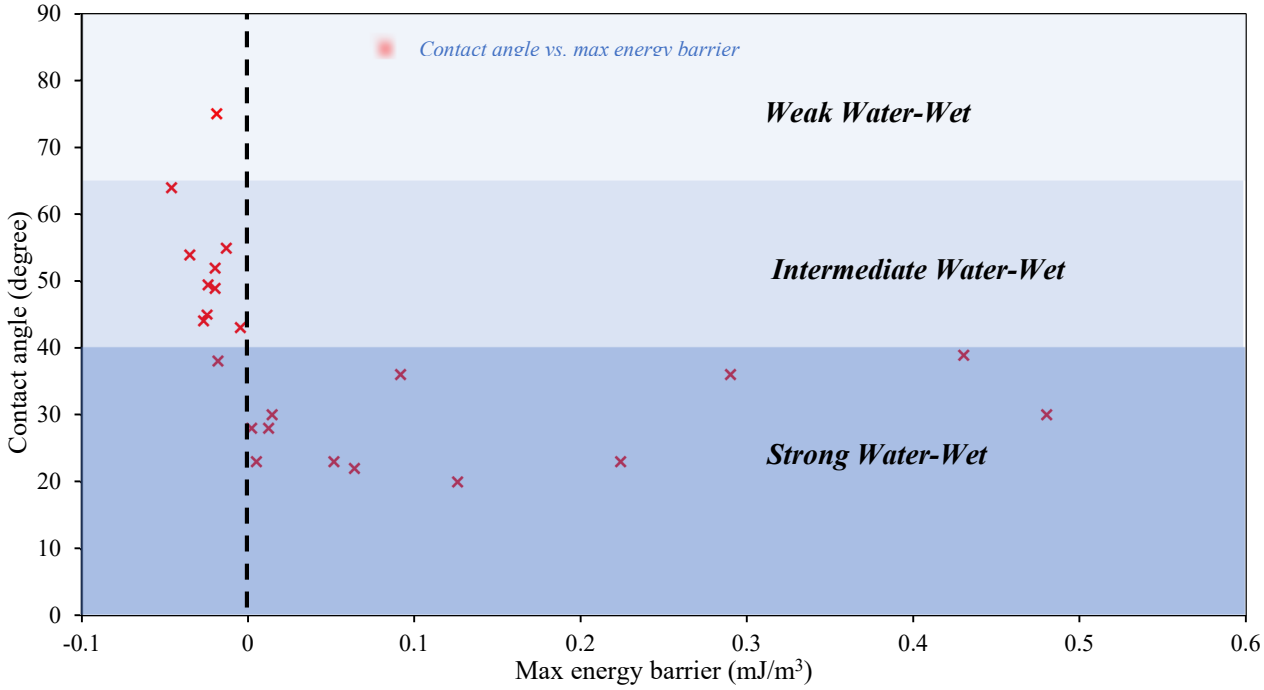

Figure 5 Correlation between experimentally measured contact angles and calculated maximum energy barrier for each contact angle [11, 17, 50, 59 – 61]

4.3 Effect of clay minerals on zeta potential and maximum energy barrier

Using the optimized modelling parameters of the different clay minerals shown in Table 1 and Table 3, the model was further employed to understand and compare the effects of the individual clay minerals on zeta potential at the rock-brine interface. The model was run for each individual clay under the same conditions. The zeta potential curve for the five clay minerals understudy is plotted against the system pH (Figure 6). The results show that smectite, montmorillonite and chlorite result in more negative zeta potential values with smectite having the highest negative zeta potential within the studied conditions. The effect of kaolinite on zeta potential is lower compared to the other three clays. Similar trend is observed for both 0.05 M NaCl (Figure 6a) and 0.005 M NaCl (Figure 6b) electrolytes. The order by which the clays affect the zeta potential is directly correlated with the site density of the surface species at clays. From Table 1, the site density at

>Al:SiOH surface for kaolinite and smectite is 11 site/nm^2 and 1.2 site/nm^2 respectively. If we compare the zeta potential curves for kaolinite and smectite in Figure 6, it is evident that in the case of kaolinite the zeta potential values are less negative than those of the smectite case. This can be attributed to the higher presence of >Al:SiOH sites on the kaolinite mineral compared to smectite, leading to a more negatively charged >Al:SiO-. These are the possible sites where the positively charged Na^+ can adsorb to. This adsorption leads to the screening of the surface charge present on the clay surface. Hence, the higher the presence of clay minerals in the sandstone rock, especially kaolinite, the more the zeta potential values at the sandstone rock-brine interface tend to be less negative. The experimental results published in [38,48] are in line with our findings. Mahani et al. [62] also highlighted that clays act as pinning points to crude oil which supports the results obtained in this study. Montmorillonite clay exhibited higher negative zeta potential values in comparison with kaolinite clay. Other studies [47,63,64] reported that the montmorillonite clay had higher negative zeta potential than kaolinite, illite and chlorite in electrolytes with different ionic strengths and over a wide range of pH. Our finding that the montmorillonite clay leads to negative zeta potential values higher than kaolinite, chlorite and illite also agrees with the published experimental results. Da Costa et al [65] measured the zeta potential for three types of sandstone: Botucatu, Berea and Bentheimer, in various electrolyte ionic strengths. Zeta potential curve shifted towards more negative values as the clay content in the sandstone rock decreased. Hence, the Bentheimer sandstone had a zeta potential curve that is more negative than the Berea sandstone, which is more negative than the Botucatu sample, exemplifying an important role of clays, as concluded in our work.

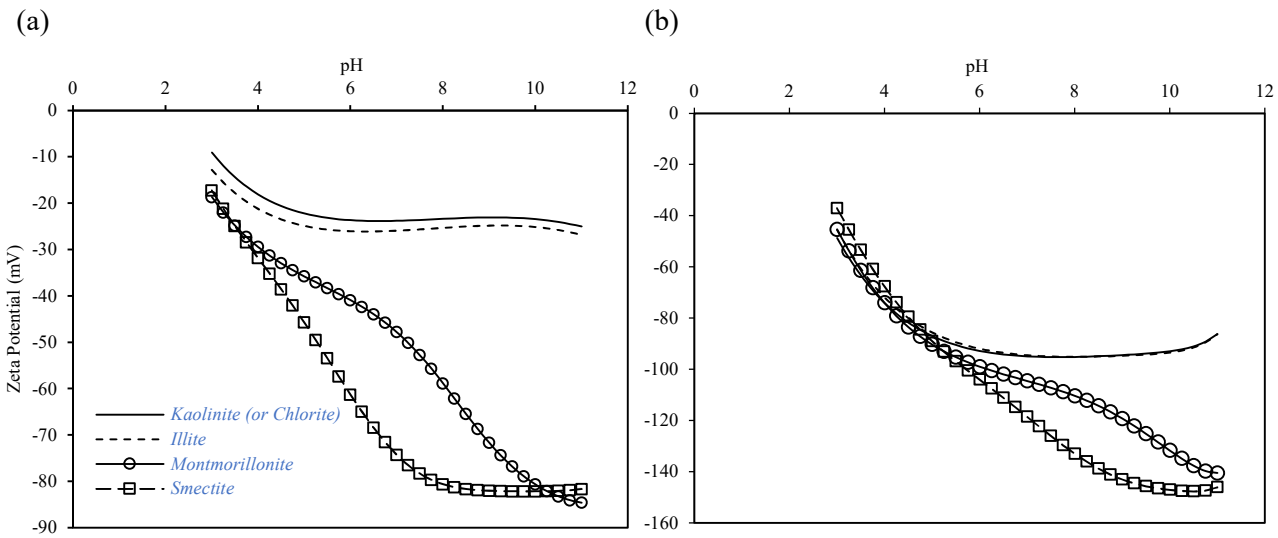

Figure 6 Zeta potential curves for different clay minerals in (a) 0.05 M NaCl electrolyte and (b) 0.005 M NaCl electrolyte

The >Al:SiOH surface site densities used are the averaged >AlOH and >SiOH site densities based on the mineral contents of the sandstone rock in question. The average >Al:SiOH surface site density affects the overall stability of the COBR system via the zeta potential at the rock-brine interface. More the negatively charged >Al:SiO-, higher will be the site density (where the cations can adsorb to), hence a less negative zeta potential at the rock-brine interface. This will lead to a lower overall disjoining pressure and interaction potential as shown in Figure 7. The results depicted in Figure 7 are in line with the findings of Bazyari et al [48] to confirm that montmorillonite exhibits disjoining pressure higher than kaolinite for several background electrolytes over a wide range of water film thickness. Based on these analyses and the MEB calculated for each clay (see Figure 8), it is concluded that the clays investigated in this study cause the zeta potential to be more negative and hence the COBR system more stable in the following order: smectite > montmorillonite > illite > chlorite > kaolinite. This implies that the higher the presence of clays that have higher >Al:SiOH site density such as kaolinite, the lower the stability of the COBR system. Borysenko et al. [66] measured the air/water contact angles of kaolinite and montmorillonite. They found that the montmorillonite clays had lower contact angles than kaolinite

clays, which is in line with the MEB results depicted in Figure 8. The rapid change in the maximum energy curve with the average rock site density demonstrates the significance of the sandstone rock mineralogy in dictating the wettability of the oil-brine-rock system.

(a)

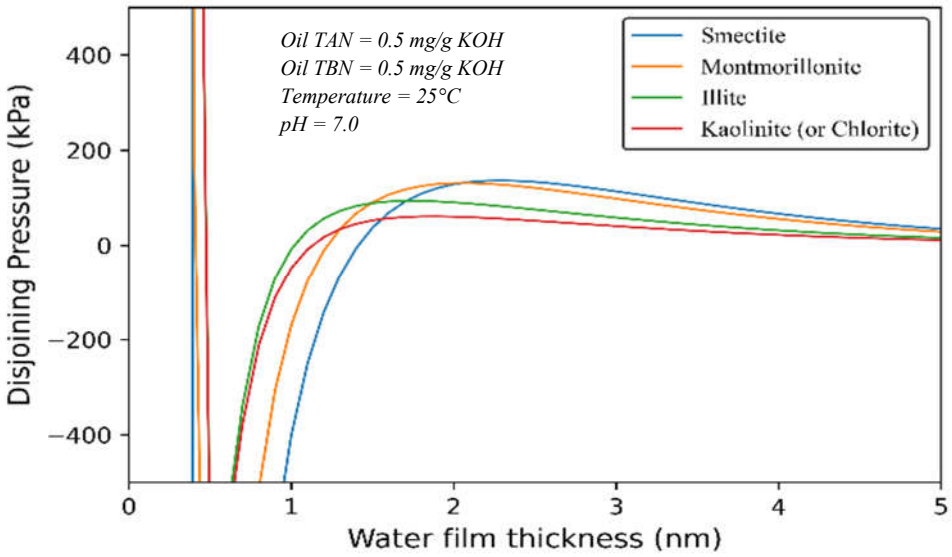

(b)

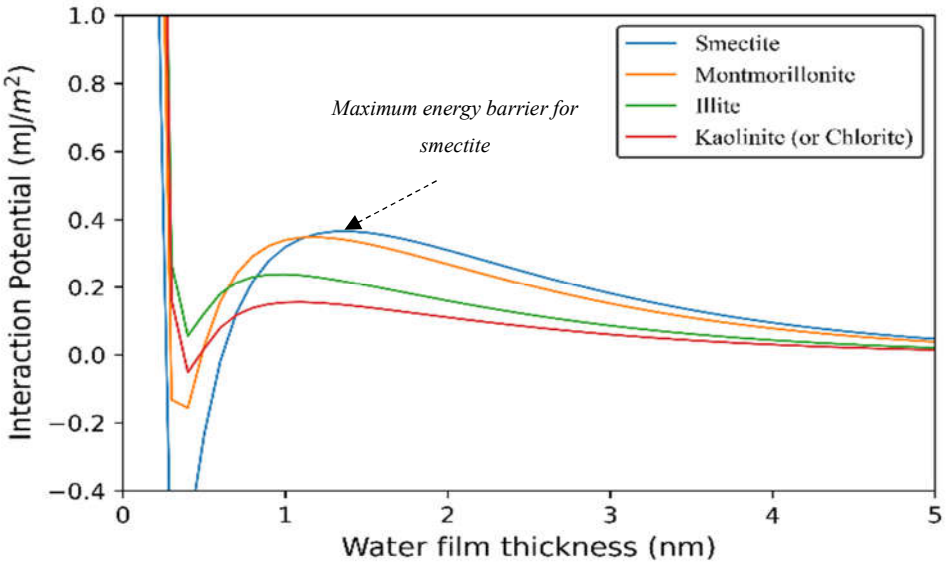

Figure 7 (a) Disjoining pressure and (b) interaction potential curves for oil-brine and rock-brine interfaces with various clay minerals

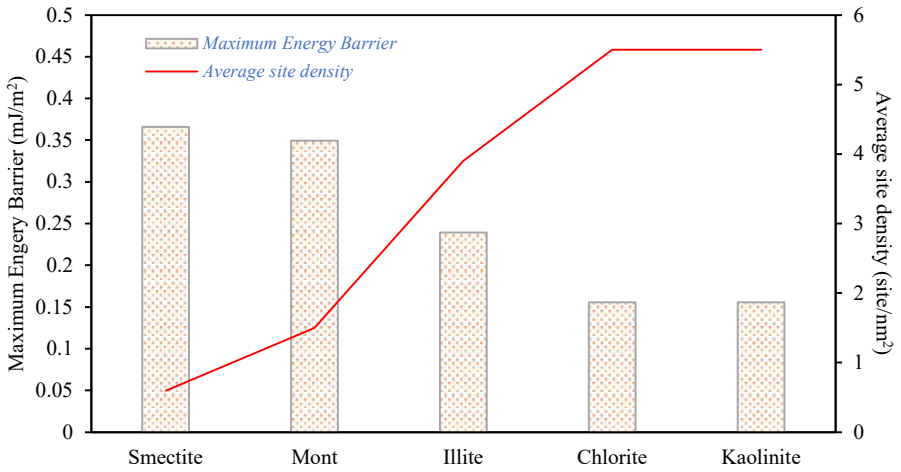

Figure 8 Maximum energy barrier variation with clay mineral type and average rock site density

4.4 Sensitivity of energy barrier to reservoir conditions and composition

Sensitivity analyses were performed to understand the contribution of various parameters in the overall stability and wettability of the COBR system. These sensitivity analyses were carried out using the workflow developed in this study, including predicting the zeta potential values using the developed TLMs followed by calculating the disjoining pressure and interaction potential energy for each studied case. Finally, the MEB was determined from the calculated interaction potential energy curves. The studied parameters include brine ionic strength, pH, temperature, rock mineralogy, oil TAN and oil TBN. The analysis was carried out by determining a base case value for each parameter, as well as minimum and maximum values to simulate the reservoir conditions of potential interest (see Table 4). Then each parameter was allowed to be changed in isolation from the other parameters between its minimum and maximum values, which allowed us to quantify the individual impact of each parameter within the studied range. The results of the sensitivity analyses are presented in Figure 9. From Figure 9, it can be clearly seen that the most important parameters that affect the reservoir wettability are the ionic strength, pH, and reservoir

440 temperature followed by the rock site density. This specific finding highlights that injection water
441 salinity is a key parameter to governing the prospects of low salinity waterflooding in sandstone
442 reservoirs. Analysis shows that increasing the salinity from 0.1 to 3 M NaCl will result in the MEB
443 reversing its sign from positive to negative, hence, shifting reservoir wettability from strong water-
444 wet to weak or intermediate water-wet conditions. The results of these analyses also highlight the
445 importance of rock mineralogy in dictating the overall reservoir wettability. By increasing the
446 average rock site density from the base value 2.5 site/nm^2 to the maximum of 5.5 site/nm^2, which
447 corresponds to the kaolinite clay site density (see Table 1), the film stability drastically drops 53%
448 from its base value 0.47 mJ/m^2. Such finding indicates that the inclusion of mineralogy is essential
449 in sandstone reservoir wettability prediction. Another interesting finding in our work is that the
450 effect of oil composition change on the overall system stability is not as pronounced as the other
451 parameters. Results show that changing the TAN of crude oil between a maximum and minimum
452 of 0.01 and 3 mg KOH/g results in a maximum of 31% change in the energy barrier. While
453 changing the TBN of a crude oil between 0 and 3 mg KOH/g results in a minimal less than 1% in
454 the energy barrier. This observation suggests that the amounts of acidic polar compounds in the
455 crude oil have a dominant effect over basic components to impact the wettability in sandstones.

456 **Table 4 Ranges of the selected parameters for sensitivity analyses**

Parameter	Base	Min	Max	Maximum energy barrier (mJ/m^2)		
				Base	Min	Max
Ionic strength (M NaCl)	0.5	0.01	3	0.47	1.7	-0.02
pH	7	5	9	0.47	-0.0068	1.154
Temperature (°C)	60	25	100	0.47	-0.018	1.095
Rock site density (site/nm^2)	5	1.2	11	0.47	0.764	0.223
TAN (mg KOH/g)	0.5	0.01	3	0.47	0.34	0.616
TBN (mg KOH/g)	0.5	0	3	0.47	0.472	0.469

457

458 We further employed our triple-layer model to evaluate the effect of continuous change of the
459 studied parameters on the overall oil-brine-sandstone system. Figure 10 compares the effects of
460 temperature and pH changes on the MEB using the base case values listed in Table 4. It can be
461 observed the increase in pH value results in a continuous increase in the energy barrier almost in a
462 linear manner (Figure 10a), which allows us to predict that an increase in pH will always result in
463 strengthening the water-wet conditions in sandstone reservoirs. This is one of the suggested
464 mechanisms of the low salinity waterflooding [7] which is also the underlying mechanism in
465 alkaline flooding. Figure 10b shows that an increase in the temperature between 25 and 100 °C, in
466 cases of using 0.5 and 1 M NaCl, results in an increase in the energy barrier from -0.02 mJ/m^2 to
467 0.53 mJ/m^2 and 1.0975 mJ/m^2, respectively. However, in the case of a 0.01 M NaCl background
468 electrolyte, the energy barrier increases from 0.695 mJ/m^2 to a maximum 1.75 mJ/m^2 at 80 °C
469 before dropping slightly to 1.6 mJ/m^2 at 100 °C. These results indicate that the pronounced effect
470 of temperature on reservoir wettability in low salinity waterflooding mostly takes place below 80
471 °C. It can also be concluded that the temperature increase beyond 80 °C - 100 °C may result in
472 reversing the wettability trend into less favourable conditions. This trend could be due to possible
473 surface overcharging, leading to a decrease in the negative surface charge and eventually reversing
474 the wettability [67].

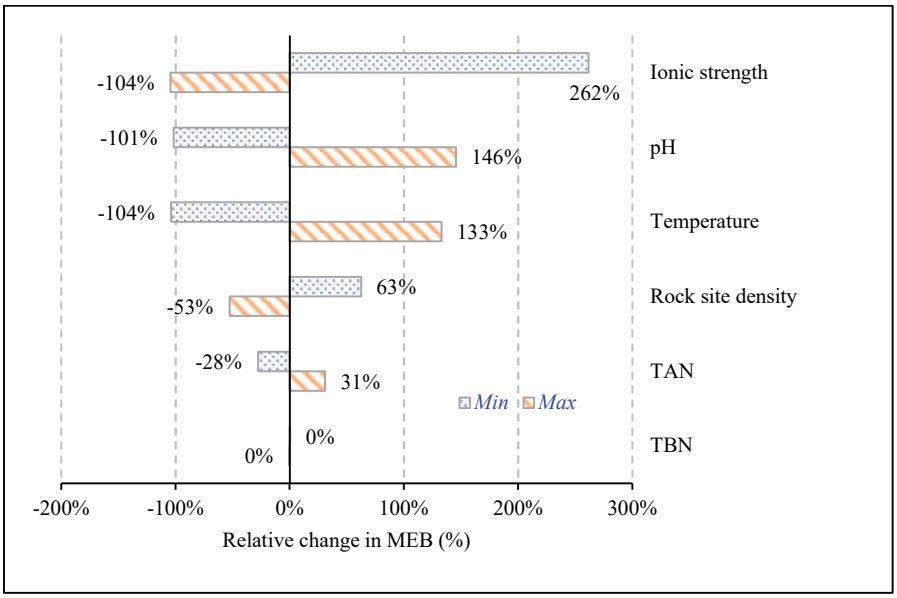

Figure 9 Relative change of maximum energy barrier against the different parameters

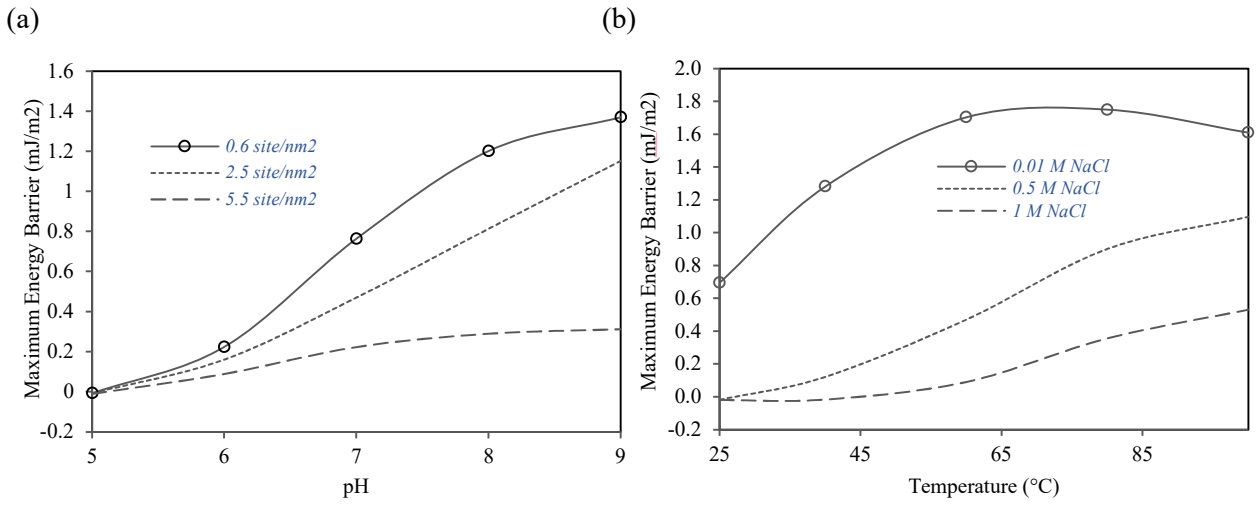

Figure 10 Sensitivity of maximum energy barrier against (a) pH at various average rock site densities and (b) temperature at various salinities

The effects of the ionic strength and average rock site density on the MEB were calculated and the results are shown in Figure 11. It shows that the increase in ionic strength of NaCl from 0.005 M to 3 M at different rock site densities results in a reduction in the MEB. It can be noticed that the effect of ionic strength on the MEB is pronounced in the range between 0.05 and 2 M NaCl where the MEB drops from 1.77 to -0.02 mJ/m^2. The energy barrier drops below the zero value when the

ionic strength increases beyond 2 M NaCl and stabilises at a maximum negative value of approximately -0.02 mJ/m^2. This implies that the target of low salinity waterflooding in a case where a reservoir with the initial conditions such as shown in Table 4 and formation water of 2 M NaCl, would be to use the injection water with a salinity less than 1 M NaCl for observing the favorable effect. Figure 11b also shows that the increase in the average rock site density has a descending effect on the oil-brine-sandstone system which is specifically evident at temperatures higher than 25°C. A high average rock site density results in more sites being available for the cations present in the brine to adsorb and screen the negative charge present on the sandstone surface. Such less negative charge results in less repulsion between the rock surface and the negatively charged oil surface leading to more oil adherence to the rock surface. This is evident quantitatively in Figure 11b for the case of 60°C temperature where the increase of average rock site density from 0.6 to 5.5 site/nm^2 leads to a drop in the MEB from 0.764 mJ/m^2 to 0.224 mJ/m^2, shifting the wettability towards less water-wet conditions.

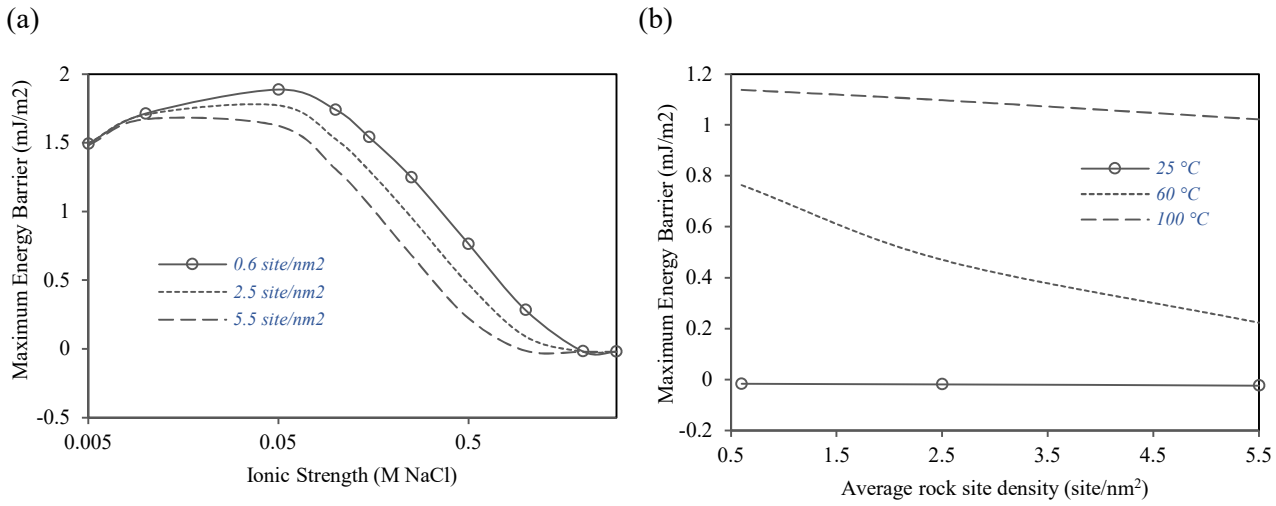

Figure 11 Sensitivity of maximum energy barrier against (a) ionic strength at various average rock site densities and (b) average rock site density at various temperatures

The impact of oil polar compounds on the MEB are depicted in Figure 12. It can clearly be seen that the effect of TAN on the MEB is more pronounced compared to TBN. This can be attributed to the fact that the TBN and positively charged amines surface groups are more present at lower

pH values where an excess of hydrogen ions associates with (-NH) to create ($-NH_2^+$). And because our studied range of pH is between 5 and 9, the effects of TBN and positively charged amine groups are not fully captured. Nevertheless, we can assume that the oil TBN does not have a pronounced effect under the usual reservoir conditions. TAN on the other hand does influence the oil-brine-sandstone system stability and wettability in reservoir conditions. Figure 12b shows that at lower salinities, an increase in the TAN results in an increase in the MEB. However, as the salinity increases and the concentration of the positive sodium ions available for adsorption increases, the increase in TAN results in a negligible change in the MEB. NaCl salinities above 1 M NaCl show a reversal in the trend where increasing the TAN leads to a very slight decrease in the MEB and hence the system stability.

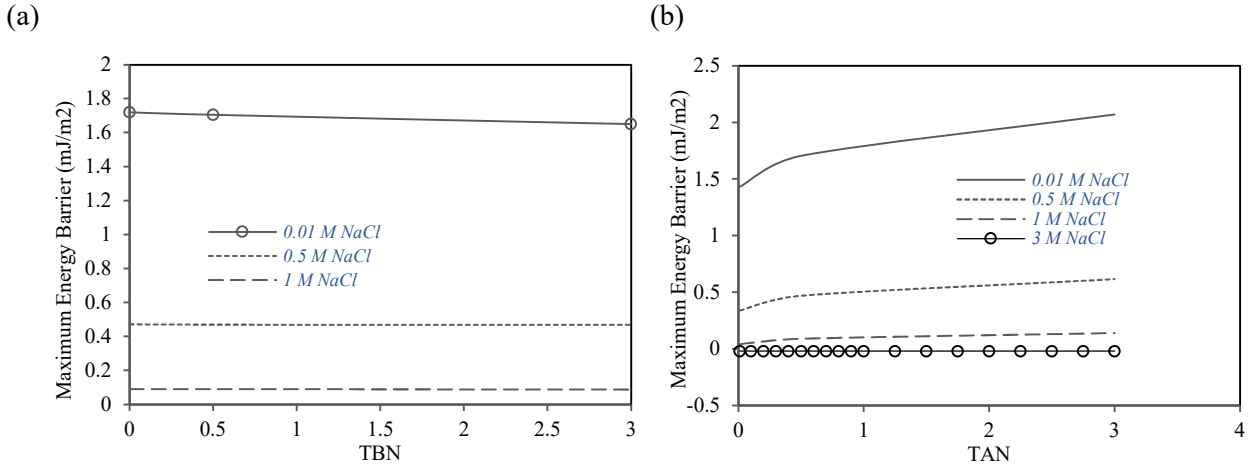

Figure 12 Sensitivity of maximum energy barrier against (a) TBN and (b) TAN at various salinities

4.5 Wettability change with reservoir conditions

In this section, the approaches used in this study are combined to quantify and provide an indicative adhesion or wettability map under the variable reservoir properties and conditions. We focus our investigation on identifying the effects of the most impactful reservoir parameters on the oil-brine-sandstone stability and wettability: pH, ionic strength, average rock site density and temperature (as discussed in the previous sections). The evaluation range of each parameter is listed in Table 4.

523 The results of these analyses were combined and summarised as wettability maps as visualised in
524 Figure 13 and Figure 14.

525 *4.5.1 Wettability map for sandstone rock in NaCl*

526 Figure 13 shows the wettability map under the various combinations of reservoir properties and
527 using NaCl as the background electrolyte in the brine. It depicts the reservoir conditions that result
528 in negative MEB that indicates weak or intermediate wetting conditions. This map demonstrates
529 the importance of salinity in determining reservoir wettability. Under almost all conditions,
530 decreasing the brine salinity resulted in an increase in the strong water-wet conditions area in the
531 map, especially, when the average rock site density is lower where the salinity effect is more
532 pronounced. This demonstrates that the main focus of LSWF in sandstone reservoirs should involve
533 reducing the brine ionic strength, which can result in shifting the reservoir wettability from
534 weak/intermediate water-wet to strongly water-wet. Another important observation is the crucial
535 role the average rock site density and clay mineralogy play in dictating the reservoir wettability.
536 The map in Figure 13 shows that having a higher site density such as 5.5 site/nm^2 causes the
537 reservoir to become weak water-wet over a wide range of reservoir conditions. This observation
538 highlights the importance of rock mineralogy in terms of composition and clay content and
539 appropriately modelling it in wettability predictions.

540 The wettability map also shows that the increase in temperature from 25 to 100 °C moves the
541 reservoir wettability towards more wetting conditions within the studied range of parameters.
542 Hence, indicating that hot low salinity waterflooding would be more beneficial under certain
543 reservoir conditions.

Temperature	*Average Ns = 0.6 site/nm²*	*Average Ns = 2.5 site/nm²*	*Average Ns = 5.5 site/nm²*
25 °C	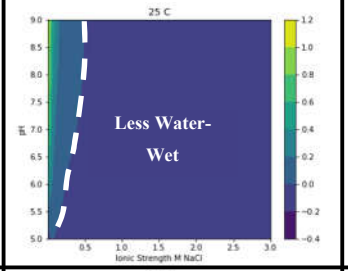	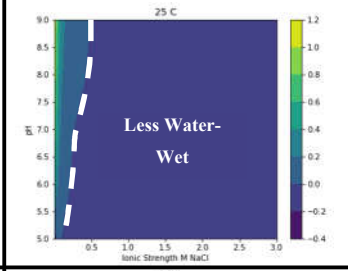	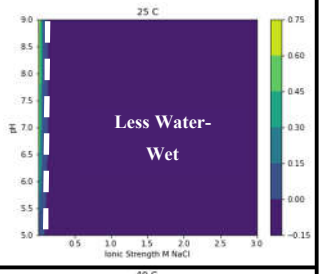
40 °C	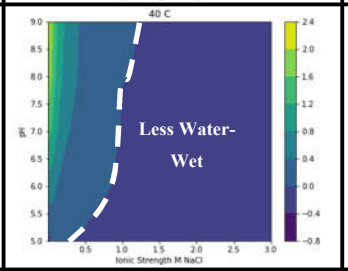	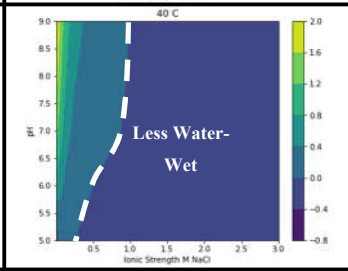	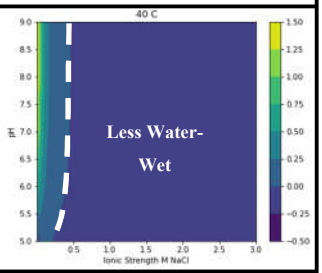
60 °C	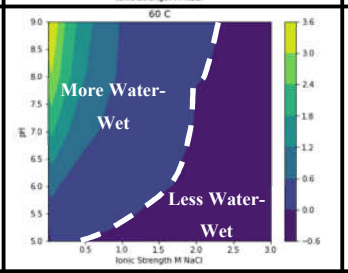	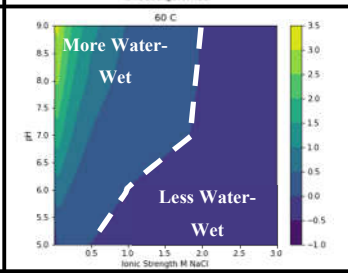	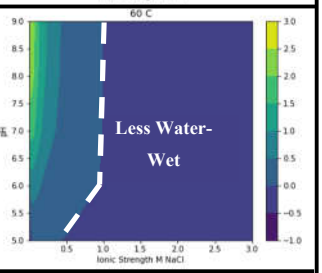
80 °C	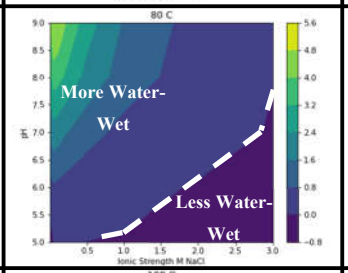	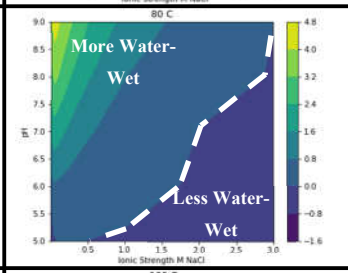	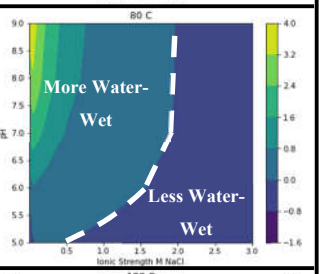
100 °C	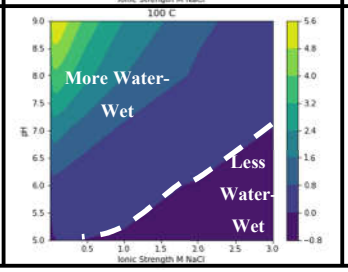	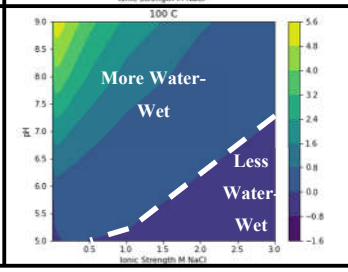	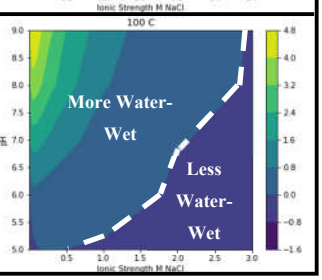

Figure 13 Wettability map against NaCl ionic strength, pH, temperature, and average rock site density

4.5.2 Wettability map for sandstone rock in $CaCl_2$

The same wettability map approach was used to evaluate the influence of the divalent cations such as Ca^{2+} in the formation brine on the reservoir wettability. The same ranges listed in Table 4 for

550 the rest of the reservoir parameters are used. The wettability map in Figure 14, demonstrates how
551 impactful the presence of the calcium ion is on the reservoir wettability in comparison with the
552 monovalent sodium ion (see Figure 13). The strong water-wet area in the adhesion map (Figure 14)
553 increases as the pH and temperature values increase which enhance the deprotonation of surface
554 sites leading to higher negative surface charge and repulsion between the two surfaces. The increase
555 in the average rock surface site density from 0.6 to 5.5 site/nm^2 suppresses the strong water-wet
556 area in the adhesion map. This can be attributed to the increase in the available surface sites for the
557 positive Ca^{2+} ions to adsorb on and screen the negative charge present at the rock surface.
558 Overall, the presence of the calcium ion significantly suppresses the areas of strong water
559 wettability under different conditions. Such finding is directly linked with the way how the calcium
560 ion affects the zeta potential at sandstone and oil-brine interfaces. Adsorption of Ca^{2+} greatly
561 reduces the negative values of the zeta potential and surface charge in comparison to sodium ion
562 thereby resulting in less electrostatic repulsion between the two interfaces. As a result, significant
563 low salinity effect and wettability alteration are expected if low salinity NaCl brine is injected into
564 sandstone reservoirs comprising of calcium-rich formation water.

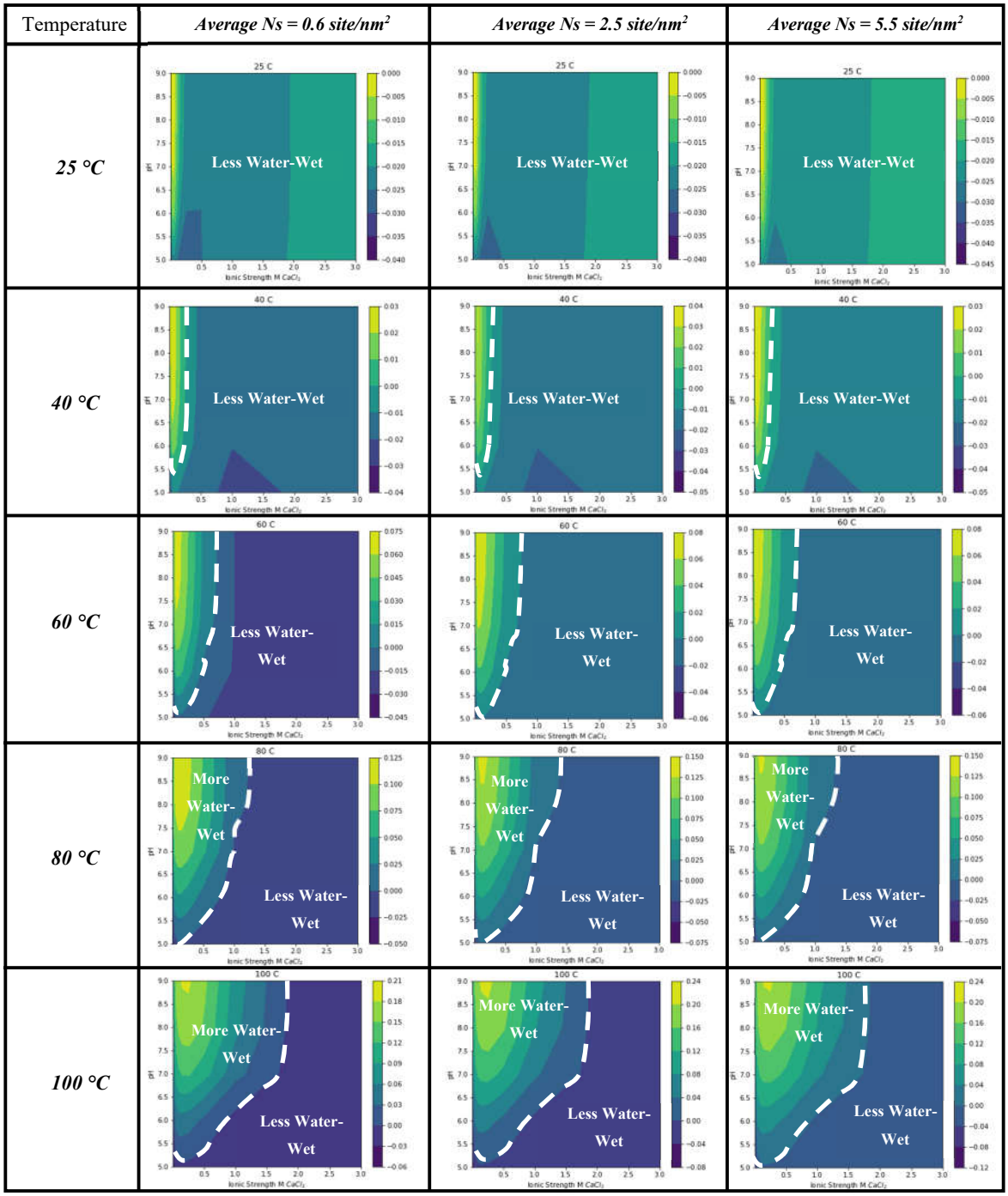

Figure 14 Wettability map against $CaCl_2$ ionic strength, pH, temperature, and average rock site density

5 Summary and Conclusions

A new sandstone-brine triple-layer surface complexation model was developed and validated against results from the published experimental studies. The developed model is the first to accommodate the individual and combined effects of sandstone minerals on the overall zeta

potential. The stability of the COBR system was analysed by calculating the disjoining pressure and interaction potential energy between the COBR interfaces using the DLVO. Furthermore, we introduced a new maximum energy barrier (MEB) concept as an indicator of reservoir wettability. The MEB was correlated well with contact angle measurements from the reported experimental studies. Analysis of the results showed that the contact angle value increases abruptly as the MEB drops below the zero-value indicating that the COBR system becomes unstable and less water-wet. This finding validates the application of maximum energy barrier concept (maximum of the interaction potential energy curve) to characterise reservoir wettability as a function of brine, oil and rock compositions, and reservoir conditions.

The developed TLM and MEB parameters were utilised to analyse the effect of sandstone mineralogy on the rock-brine zeta potential and reservoir wettability. The presence of kaolinite in the sandstone reservoir causes the COBR system to become less stable and less water-wet in comparison with the other studied clay minerals i.e. chlorite, illite, montmorillonite and smectite. Further sensitivity analysis indicated that the brine composition is the most impacting parameter on reservoir wettability amongst the investigated parameters. The importance of different studied parameters on reservoir wettability in sandstones was found to be in the following order: ionic strength and brine composition > pH > temperature > sandstone mineralogy > oil TAN > oil TBN. Furthermore, the rapid change in the maximum energy curve with the average rock site density demonstrates the significance of the sandstone rock mineralogy in dictating the wettability of the oil-brine-sandstone system. Also, the presence of $CaCl_2$ in the formation water significantly suppresses the areas of strong water wettability under different reservoir conditions compared to NaCl.

The modelling work conducted in this research is limited to the types of clay considered in the sandstone-brine triple-layer model i.e. kaolinite, chlorite, illite, montmorillonite and smectite. Other clays and minerals may also be present in a sandstone rock. Moreover, the validation range

of the data used for optimising the developed oil-brine and sandstone-brine models is between 50 and 175,000 ppm for brine salinity, between 25 and 65 °C for temperatures and 2 – 11 pH. The application of the developed workflow was also extended outside these validation ranges to gain valuable insights into how these different parameters affect sandstone wettability. Nonetheless, the workflow presented in this study will provide useful practical guidelines in screening sandstone reservoir candidates for potential low salinity waterflooding applications.

6 Abbreviations and Nomenclature

6.1 Abbreviations

CD-MUSIC	Charge-distribution multisite surface complexation
COBR	Crude oil-brine-rock
DLVO	Derjaguin, Landau, Verwey, and Overbeek
LSE	Low salinity effect
LSWF	Low salinity waterflooding
MEB	Maximum energy barrier
MIE	Multicomponent ion exchange
PDIs	Potential determining ions
SCM	Surface complexation modelling
TAN	Total acid number
TBN	Total base number
TLM	Triple-layer surface complexation models

VdW	Van der Waal

605

606 **6.2 Nomenclature**

A	Hamaker constant
$A_{v=0},\ A_{v>0}$	Contributions to Hamaker constant at zero and finite frequencies
A_s	Structural force coefficient
C_1, C_2	Capacitances of the inner and outer Helmholtz layers
d	Thickness of the layer
e	Electron charge
F	Faraday constant
h	Distance between the two interfaces
I	Ionic strength of the solution
k_B	Boltzmann constant
MW_{KOH}	Molecular weight of KOH
n_1, n_2, n_3	Refractive indexes for medium 1, 2, 3
N_A	Avogadro's number
n_b	Ion density in the bulk solution
N_s	Surface site density
T	Temperature
x	Distance away from the surface in meters
ε_0	Dielectric constant of free space
ε	Relative dielectric constant
ζ	Zeta potential

κ	Debye-Huckel parameter
λ_{lw}	London wavelength
$\Pi(h)$	Disjoining pressure
$\Pi_{electric}(h)$	Electrostatic forces
$\Pi_{structural}(h)$	Structural forces
$\Pi_{VdW}(h)$	Van der Waals forces
ρ	Ionic concentration
σ	Charge density
ψ	Potential
ψ_r	Reduced surface potential

7 References

[1] J.J. Sheng, Critical review of low-salinity waterflooding, Journal of Petroleum Science and Engineering. 120 (2014) 216-224.

[2] S.C. Ayirala and A.A.Yousef, A state-of-the-art review to develop injection-water-chemistry requirement guidelines for IOR/EOR projects. SPE Production & Operations, 30(01), (2015)_pp.26-42.

[3] S.O. Olayiwola and M. Dejam, A comprehensive review on interaction of nanoparticles with low salinity water and surfactant for enhanced oil recovery in sandstone and carbonate reservoirs. Fuel, 241, (2019) pp.1045-1057.

[4] S.O. Olayiwola and M. Dejam, Synergistic interaction of nanoparticles with low salinity water and surfactant during alternating injection into sandstone reservoirs to improve oil recovery and reduce formation damage. Journal of Molecular Liquids, 317, (2020) p.114228.

[5] S. Ayirala, A. AlSofi, Z. AlYousef, J. Wang, M.A. Alsaud and A. AlYousef, SmartWater based synergistic technologies for enhanced oil recovery. Fuel, 316, (2022) p.123264.

[6] D.J. Ligthelm, J. Gronsveld, J. Hofman, N. Brussee, F. Marcelis, H. van der Linde, Novel waterflooding strategy by manipulation of injection brine composition. (2009).

[7] P. McGuire, J. Chatham, F. Paskvan, D. Sommer, F. Carini, Low salinity oil recovery: An exciting new EOR opportunity for Alaska's North Slope, (2005).

[8] G. Tang, N.R. Morrow, Influence of brine composition and fines migration on crude oil/brine/rock interactions and oil recovery, Journal of petroleum science and engineering. 24 (1999) 99-111.

[9] A. Lager, K.J. Webb, C. Black, M. Singleton, K.S. Sorbie, Low salinity oil recovery-an experimental investigation1, Petrophysics-The SPWLA Journal of Formation Evaluation and Reservoir Description. 49 (2008).

[10] J. Buckley, N. Morrow, Improved oil recovery by low salinity waterflooding: A mechanistic review, (2010) 6-9.

[11] R.A. Nasralla, H.A. Nasr-El-Din, Double-layer expansion: is it a primary mechanism of improved oil recovery by low-salinity waterflooding? SPE Reservoir Evaluation & Engineering. 17 (2014) 49-59.

[12] A.N. Awolayo, H.K. Sarma, L.X. Nghiem, Brine-dependent recovery processes in carbonate and sandstone petroleum reservoirs: review of laboratory-field studies, interfacial mechanisms and modeling attempts. Energies, 11 (2018) p.3020.

[13] P.V. Brady, J.L. Krumhansl, A surface complexation model of oil–brine–sandstone interfaces at 100 C: Low salinity waterflooding, Journal of Petroleum Science and Engineering. 81 (2012) 171-176.

[14] S. Erzuah, I. Fjelde, A.V. Omekeh, Wettability estimation by surface complexation simulations, (2017).

[15] Y. Elakneswaran, M. Shimokawara, T. Nawa, S. Takahashi, Surface complexation and equilibrium modelling for low salinity waterflooding in sandstone reservoirs, (2017).

[16] Q. Xie, F. Liu, Y. Chen, H. Yang, A. Saeedi, M.M. Hossain, Effect of electrical double layer and ion exchange on low salinity EOR in a pH controlled system, Journal of Petroleum Science and Engineering. 174 (2019) 418-424.

[17] Q. Xie, P.V. Brady, E. Pooryousefy, D. Zhou, Y. Liu, A. Saeedi, The low salinity effect at high temperatures, Fuel. 200 (2017) 419-426.

[18] R. Khaledialidusti, J. Kleppe, Surface-charge alteration at the carbonate/brine interface during single-well chemical-tracer tests: Surface-complexation model, SPE Journal. 23 (2018) 2302-2315.

[19] E. Pooryousefy, Q. Xie, Y. Chen, A. Sari, A. Saeedi, Drivers of low salinity effect in sandstone reservoirs, Journal of Molecular Liquids. 250 (2018) 396-403.

[20] H. Sharma, K.K. Mohanty, An experimental and modeling study to investigate brine-rock interactions during low salinity water flooding in carbonates, Journal of Petroleum Science and Engineering. 165 (2018) 1021-1039.

[21] Y. Chen, Q. Xie, A. Saeedi, Role of ion exchange, surface complexation, and albite dissolution in low salinity water flooding in sandstone, Journal of Petroleum Science and Engineering. 176 (2019) 126-131.

[22] N. Kallay, D. Kovačević, S. Žalac, Thermodynamics of the solid/liquid interface-its application to adsorption and colloid stability, in: Anonymous Interface Science and Technology, Elsevier, 2006, pp. 133-170.

[23] A.R. Vieira, Surface Complexation Modeling of Lead (II), Cadmium (II) and Selenium (IV) Onto Iron Hydroxides in Single and Bisolute Systems, The University of Texas at Austin, 2006.

[24] M. Villalobos, Triple layer modelling of carbonate adsorption on goethites with variable adsorption capacities based on congruent site-occupancy, in: Anonymous Interface Science and Technology, Elsevier, 2006, pp. 417-442.

[25] M. Takeya, A. Ubaidah, M. Shimokawara, H. Okano, T. Nawa, Y. Elakneswaran, Crude oil/brine/rock interface in low salinity waterflooding: Experiments, triple-layer surface complexation model, and DLVO theory, Journal of Petroleum Science and Engineering. 188 (2020) 106913.

[26] M. Takeya, M. Shimokawara, Y. Elakneswaran, H. Okano, T. Nawa, Effect of acid number on the electrokinetic properties of crude oil during low-salinity waterflooding, Energy Fuels. 33 (2019) 4211-4218.

[27] F. Liu, M. Wang, Electrokinetic Mechanisms and Synergistic Effect on Ion-Tuned Wettability in Oil-Brine-Rock Systems, Transp. Porous Media. (2021) 1-20.

[28] M. Takeya, M. Shimokawara, Y. Elakneswaran, T. Nawa, S. Takahashi, Predicting the electrokinetic properties of the crude oil/brine interface for enhanced oil recovery in low salinity water flooding, Fuel. 235 (2019) 822-831.

[29] J.T. Tetteh, A. Pham, E. Peltier, J.M. Hutchison, R.B. Ghahfarokhi, Predicting the electrokinetic properties on an outcrop and reservoir composite carbonate surfaces in modified salinity brines using extended surface complexation models, Fuel. 309 (2022) 122078.

[30] M. Taheriotaghsara, M. Bonto, H.M. Nick, A.A. Eftekhari, Estimation of calcite wettability using surface forces, Journal of Industrial and Engineering Chemistry. 98 (2021) 444-457.

[31] M. Bonto, A.A. Eftekhari, H. M. Nick, Wettability Indicator Parameter Based on the Thermodynamic Modeling of Chalk-Oil-Brine Systems, Energy Fuels. 34 (2020) 8018-8036.

[32] P.V. Brady, N.R. Morrow, A. Fogden, V. Deniz, N. Loahardjo, Electrostatics and the low salinity effect in sandstone reservoirs, Energy Fuels. 29 (2015) 666-677.

[33] P. Leroy, A. Revil, A triple-layer model of the surface electrochemical properties of clay minerals, J. Colloid Interface Sci. 270 (2004) 371-380.

[34] O.L. Gaskova, M.B. Bukaty, Sorption of different cations onto clay minerals: modelling approach with ion exchange and surface complexation, Physics and Chemistry of the Earth, Parts A/B/C. 33 (2008) 1050-1055.

[35] M. Saeed, P. Jadhawar, Y. Zhou, R. Abhishek, Triple-Layer Surface Complexation Modelling: Characterization of Oil-Brine Interfacial Zeta Potential Under Varying Conditions of Temperature,

pH, Oil Properties and Potential Determining Ions, Colloids Surf. Physicochem. Eng. Aspects. (2022) 127903.

[36] A. Hurst, J. Archer, Sandstone reservoir description: An overview of the role of geology and mineralogy, Clay Miner. 21 (1986) 791-809.

[37] G. Hirasaki, Wettability: fundamentals and surface forces, SPE Form. Eval. 6 (1991) 217-226.

[38] N. Vdović, I. Jurina, S.D. Škapin, I. Sondi, The surface properties of clay minerals modified by intensive dry milling—revisited, Appl. Clay. Sci. 48 (2010) 575-580.

[39] Q. Du, Z. Sun, W. Forsling, H. Tang, Acid–base properties of aqueous illite surfaces, J. Colloid Interface Sci. 187 (1997) 221-231.

[40] E. Tertre, S. Castet, G. Berger, M. Loubet, E. Giffaut, Surface chemistry of kaolinite and Na-montmorillonite in aqueous electrolyte solutions at 25 and 60 C: Experimental and modeling study, Geochim. Cosmochim. Acta. 70 (2006) 4579-4599.

[41] J.M. Zachara, J.P. McKinley, Influence of hydrolysis on the sorption of metal cations by smectites: Importance of edge coordination reactions, Aquat. Sci. 55 (1993) 250-261.

[42] M. Hasegawa, M. Kimata, M. Shimane, T. Shoji, M. Tsuruta, The effect of liquid additives on dry ultrafine grinding of quartz, Powder Technol. 114 (2001) 145-151.

[43] P.W. Glover, E. Walker, M.D. Jackson, Streaming-potential coefficient of reservoir rock: A theoretical model, Geophysics. 77 (2012) D17-D43.

[44] J.N. Israelachvili, Intermolecular and Surface Forces, Academic press, 2015.

[45] D.L. Parkhurst, C. Appelo, Description of input and examples for PHREEQC version 3: a computer program for speciation, batch-reaction, one-dimensional transport, and inverse geochemical calculations. (2013).

[46] U. Farooq, M.T. Tweheyo, J. Sjöblom, G. Øye, Surface characterization of model, outcrop, and reservoir samples in low salinity aqueous solutions, J. Dispersion Sci. Technol. 32 (2011) 519-531.

[47] X. Quan, W. Jiazhong, Q. Jishun, L. Qingjie, M. Desheng, L. Li, L. Manli, Investigation of electrical surface charges and wettability alteration by ions matching waterflooding, (2012) 27-30.

[48] A. Bazyari, B.S. Soulgani, M. Jamialahmadi, A. Dehghan Monfared, A. Zeinijahromi, Performance of smart water in clay-rich sandstones: experimental and theoretical analysis, Energy Fuels. 32 (2018) 10354-10366.

[49] C. Chassagne, F. Mietta, J. Winterwerp, Electrokinetic study of kaolinite suspensions, J. Colloid Interface Sci. 336 (2009) 352-359.

[50] Q. Xie, Y. Liu, J. Wu, Q. Liu, Ions tuning water flooding experiments and interpretation by thermodynamics of wettability, Journal of Petroleum Science and Engineering. 124 (2014) 350-358.

[51] M.B. Alotaibi, R.A. Nasralla, H.A. Nasr-El-Din, Wettability studies using low-salinity water in sandstone reservoirs, SPE Reservoir Evaluation & Engineering. 14 (2011) 713-725.

[52] Y. Yukselen-Aksoy, A. Kaya, A study of factors affecting on the zeta potential of kaolinite and quartz powder, Environmental Earth Sciences. 62 (2011) 697-705.

[53] A. Kaya, A.H. Oren, Y. Yukselen, Settling behavior and zeta potential of kaolinite in aqueous media, (2003).

[54] W. Van Riemsdijk, T. Hiemstra, The CD-MUSIC model as a framework for interpreting ion adsorption on metal (hydr) oxide surfaces, in: Anonymous Interface Science and Technology, Elsevier, 2006, pp. 251-268.

[55] J. Gregory, Approximate expressions for retarded van der Waals interaction, J. Colloid Interface Sci. 83 (1981) 138-145.

[56] R.J. Hunter, L.R. White, D.Y.C. Chan, Foundations of Colloid Science, Clarendon Press, 1987.

[57] J. Buckley, K. Takamura, N. Morrow, Influence of electrical surface charges on the wetting properties of crude oils, SPE reservoir engineering. 4 (1989) 332-340.

[58] M. Sadeqi-Moqadam, S. Riahi, A. Bahramian, An investigation into the electrical behavior of oil/water/reservoir rock interfaces: The implication for improvement in wettability prediction, Colloids Surf. Physicochem. Eng. Aspects. 490 (2016) 268-282.

[59] H. Reerink, J.T.G. Overbeek, The rate of coagulation as a measure of the stability of silver iodide sols, Discuss. Faraday Soc. 18 (1954) 74-84.

[60] E.V. Lebedeva, A. Fogden, Adhesion of oil to kaolinite in water, Environ. Sci. Technol. 44 (2010) 9470-9475.

[61] J.V. Nicolini, H.C. Ferraz, C.P. Borges, Effect of seawater ionic composition modified by nanofiltration on enhanced oil recovery in Berea sandstone, Fuel. 203 (2017) 222-232.

[62] H. Mahani, S. Berg, D. Ilic, W. Bartels, V. Joekar-Niasar, Kinetics of the low salinity waterflooding effect studied in a model system, (2013).

[63] I. Sondi, J. Bišćan, V. Pravdić, Electrokinetics of pure clay minerals revisited, J. Colloid Interface Sci. 178 (1996) 514-522.

[64] R.A. Nasralla, H.A. Nasr-El-Din, Impact of cation type and concentration in injected brine on oil recovery in sandstone reservoirs, Journal of Petroleum Science and Engineering. 122 (2014) 384-395.

[65] A.A. da Costa, J. Soares, P. Rocha, G. Costa, M. Embiruçu, An experimental evaluation of low salinity water mechanisms in a typical Brazilian sandstone and light crude oil with low acid/basic number, Fuel. 273 (2020) 117694.

766 [66] A. Borysenko, B. Clennell, R. Sedev, I. Burgar, J. Ralston, M. Raven, D. Dewhurst, K. Liu,
767 Experimental investigations of the wettability of clays and shales, Journal of Geophysical
768 Research: Solid Earth. 114 (2009).

769 [67] Z.Y. Wang, P. Zhang, Z. Ma, On the physics of both surface overcharging and charge
770 reversal at heterophase interfaces. Physical Chemistry Chemical Physics, 20(6) (2018), pp.4118-
771 4128.